Available online at www.sciencedirect.com
ScienceDirect
Catalysis Today 118 (2006) 323–331
CATALYSIS TODAY
www.elsevier.com/locate/cattod

In situ TPR/TPO-Raman studies of dispersed and nano-scaled mixed V-Nb oxides on alumina

Anna E. Lewandowska, Miguel A. Bañares *

Instituto de Catálisis y Petroleoquímica, CSIC, Marie Curie 2, E-28049 Madrid, Spain

Available online 17 August 2006

Abstract

Various catalysts containing niobium and vanadium oxides supported on alumina were prepared by wet impregnation via aqueous solution using several precursors. The total loading of V and Nb oxides were below their dispersion limit on alumina. Vanadyl sulfate, ammonium metavanadate and ammonium niobate(V) oxalate were the precursors for supported vanadia and niobia. The reduction/oxidation properties were studied by conventional TPR/TPO and TPR/TPO-Raman. Surface vanadium oxide species tend to increase their polymerization degree upon TPR/TPO cycles. A broad weak feature near 900 cm^{-1} appears associated to V^{3+}–O–Al^{3+} bond vibration in the reduced vanadia-alumina catalysts. Niobia appears to retard vanadia reduction. Regarding supported niobia, a fraction of surface niobia is significantly more reducible than surface vanadia and another fraction is significantly less reducible. The more reducible niobia appears associated to an incipient Nb–Al–O phase that may account for a fluorescence background observed in the Raman spectra. The less reducible niobia phases appears associated to dispersed niobium oxide species on alumina. Niobium has an effect on vanadia reduction profiles in VNb/Al_2O_3 system.

Keywords: Supported vanadia-niobia; Alumina; TPR-Raman; TPO-Raman; *In situ*

1. Introduction

Supported metal oxides are widely used in many industrial applications. Vanadium containing catalysts are applied in the catalytic oxidation reaction. It is a unique element that may catalyze chemical processes by formation oxo- or peroxo intermediate complex. The form of this complex depends on the catalytic conditions [1]. In the catalytic systems vanadium is mostly supported or incorporated into the framework of molecular sieves [2–4]. The properties of vanadium-based catalysts are further tuned by the use of a second element. The catalytic properties of supported mixed metal oxides (Sb + V [5], Mo + V [6]) are studied in the oxidation processes. The progress concerns also the systems possess mixed V + Nb bulk oxides, supported mixed metal oxides [7–9] as well as vanadium-niobium-containing molecular sieves [10]. Niobium compounds exhibit properties different from those of the surrounding elements of niobium in the periodic table [11,12] and they are used in the catalytic systems either as a promoter or as a support [11–13]. The addition of Nb affects properties of catalytic material, like their reducibility, acidity or photosensitivity.

2. Experimental

2.1. Preparation of samples

The vanadium and niobium oxides supported on alumina were prepared using different V precursors. *Vanadia on alumina* catalysts were prepared from an aqueous solution of $VOSO_4$ (Aldrich, 99.99%), which was kept under stirring at 323 K for 50 min. Then γ-Al_2O_3 (SASOL, S_{BET} = 193 $m^2\ g^{-1}$) was added. The resulting suspension was evaporated in a rotatory evaporator at 338 K. The resulting solid was dried at 388 K for 20 h and then calcined at 673 K for 4 h in air. The rate of the heating was 5 K min^{-1}. The preparation of alumina supported V-Nb and Nb oxides uses NH_4VO_3 (Sigma, 99.99%) and $C_4H_4NNbO_9$ (Aldrich, 99.99%) solutions. Oxalic acid (Panreac, 99.5%) was added to the aqueous solution of ammonium metavanadate and ammonium niobate(V) oxalate to facilitate dissolving the salts. Oxalic acid was also used for the impregnation procedure of niobium on alumina. The monolayer value – understood as the dispersion limit loading of

* Corresponding author. Tel.: +34 915854788; fax: +34 915854860.
E-mail address: banares@icp.csic.es (M.A. Bañares).

0920-5861/$ – see front matter © 2006 Elsevier B.V. All rights reserved.
doi:10.1016/j.cattod.2006.07.014

the supported oxides – was estimated as a total number of eight atoms (V + Nb)/nm^2 of alumina support. The amount of V, Nb and V + Nb was calculated so that a total coverage of metals would correspond to 1/2 and 3/4 of the monolayer value. The V/Nb atomic ratio was fixed to 1. The general *x*V/Al, *x*Nb/Al and *x*VNb/Al nomenclature was applied, where "*x*" indicates the number of atoms per nm^2 of V and Nb. The V_2O_5 and Nb_2O_5 loadings were determined by X-ray fluorescence.

2.2. Characterization

X-ray diffraction patterns were recorded by Siemens Kristalloflex D-500 diffractometer with Cu Kα radiation (λ = 1.54059 Å) and the graphite monochromator. The measurement was carried out in the 2Θ angle range from 5° to 90° and a step size 0.04°/s.

Temperature-programmed reduction and oxidation (TPR/TPO) were performed in a fixed-bed quartz reactor with a Micromeritics TPD/TPR 2900 analyzer. The reduction of the samples was carried out using H_2/Ar (10 vol.%) as reductant (flow rate = 40 cm^3 min^{-1}). A 30 mg of the samples placed in the reactor were activated in a flow of synthetic air at 673 K at a rate of 5 K min^{-1}. After the sample was cooled to RT in synthetic air, then, it was heated at a rate of 10 K min^{-1} to 1323 K under the reducing feed. After the reduction experiment (H_2-TPR) the sample was cooled to RT in He. O_2/He mixture was used as an oxidant (flow rate = 75 cm^3 min^{-1}) in the temperature-programmed oxidation (TPO). The oxidation of the materials was performed from 313 to 1223 K at a rate of 10 K min^{-1}. A thermal conductivity detector measured hydrogen and oxygen consumption. The Nb_2O_5 (CBMM) and V_2O_5 (Fluka, 99%) were used as bulk oxides pattern in the TPR measurement.

Raman spectra were run with a single monochromator Renishaw System-1000 microscope Raman equipped with a cooled CCD detector (200 K) and holographic super-Notch filter. The holographic Notch filter removes the elastic scattering while the Raman signal remains high. The powder samples were excited with the 514 nm Ar^+ line; spectral resolution was near 3 cm^{-1} and spectra acquisition consisted of 20 accumulations of 10 s. The spectra were obtained under reductive and oxidative conditions (TPR- and TPO-Raman, respectively) in a hot stage (Linkam TS-1500). Prior to the reduction experiment, the catalysts were dehydrated in synthetic air flow at 673 K at a rate of 5 K min^{-1}. After the sample was cooled to RT in synthetic air, the reduction of the materials was carried out from 303 to 1023 K in a flow of 1 vol.% H_2 in Ar (SEO-L'Air Liquide) at 10 K min^{-1}. After the reduction the sample was cooled to RT under the reducing mixture. Then, it was heated at 10 K min^{-1} to 1023 K under the flow of synthetic air. The oxidized catalyst was cooled to RT under the oxidizing mixture. The spectra of hydrated samples were obtained at room temperature in a flow of humid air.

3. Results

The *XRD analyses* of the catalysts are shown in Fig. 1. All materials exhibit similar diffraction patterns, which correspond to alumina support (γ-Al_2O_3, JCPDS file 10–425) (Fig. 1). These results indicate that vanadium and niobium oxides below monolayer coverage are essentially dispersed on the support, within the detection limits of XRD: small crystallites (<4 nm) cannot generate X-ray diffraction patterns [14,15]. The XRD pattern for 6V/Al (XRD pattern not shown) exhibits a diffraction peak at 25.52° that is not visible in 4V/Al. It can be attributed to V_6O_{13} phase (JCPDS file 19-1399), $AlVO_4$ phase (JCPDS file 31-34) or VO_2 phase (JCPDS file 31-1439). No diffraction pattern of Nb- or V-containing phases is detected.

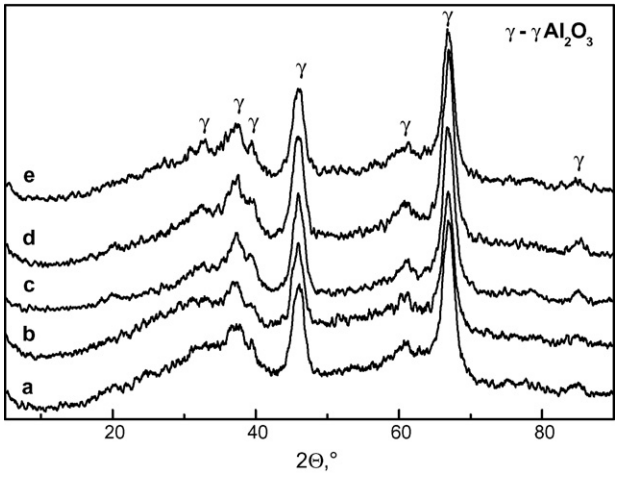

Fig. 1. XRD patterns of alumina supported vanadium and niobium catalysts: (a) 4Nb/Al, (b) 6Nb/Al, (c) 4V/Al, (d) 4VNb/Al and (e) 6VNb/Al.

Fig. 2 illustrates the H_2-TPR profiles of the pure Nb_2O_5 and V_2O_5 oxides (dashed lines) and those corresponding to alumina-supported catalysts (solid lines). The onset reduction temperature ($T_{o,red}$) and the temperature of peak maximum (T_{Mi}) are summarized in Table 1. Fig. 2A illustrates the TPR profiles for the niobia series. The onset reduction temperatures for 4Nb/Al, 6Nb/Al and bulk Nb_2O_5 (Table 1) fall in the 315–390 K range. 4Nb/Al and 6Nb/Al exhibit low-temperature reduction profiles similar to that of bulk Nb_2O_5. In the low-temperature (LT) region, a broad peak reaches its maximum at 558 and 567 K (T_{M2}). Bulk Nb_2O_5 reduces at higher temperatures (614 K), which is consistent with previous studies [16]. This shift in the LT reduction temperature may evidence the presence niobium species that are easier to reduce than bulk Nb_2O_5. Quite a different trend is observed for the HT reduction peak; which is the main reduction peak of bulk niobia (Fig. 2A). According to the literature [17], the maximum at 1117 K (T_{M4}) corresponds to a reduction of Nb^{5+} to Nb^{4+} in bulk niobia. The profiles (a) and (b) illustrate a dramatic increase in the reduction temperature for the HT peak up to 1278 K in 6Nb/Al and above this value for 4Nb/Al, where the reduction process is not complete in our experimental conditions. Alumina-supported niobia reduces above 1200 K (T_{M4}). This maximum approaches that of bulk niobia with coverage. Thus, the niobia-alumina interaction appears to stabilize niobia against reduction by more than 100 K; on the other hand, it also facilitates the reduction of another fraction of niobia species (LT peak). There must clearly be two kinds of niobia species formed upon interaction with alumina.

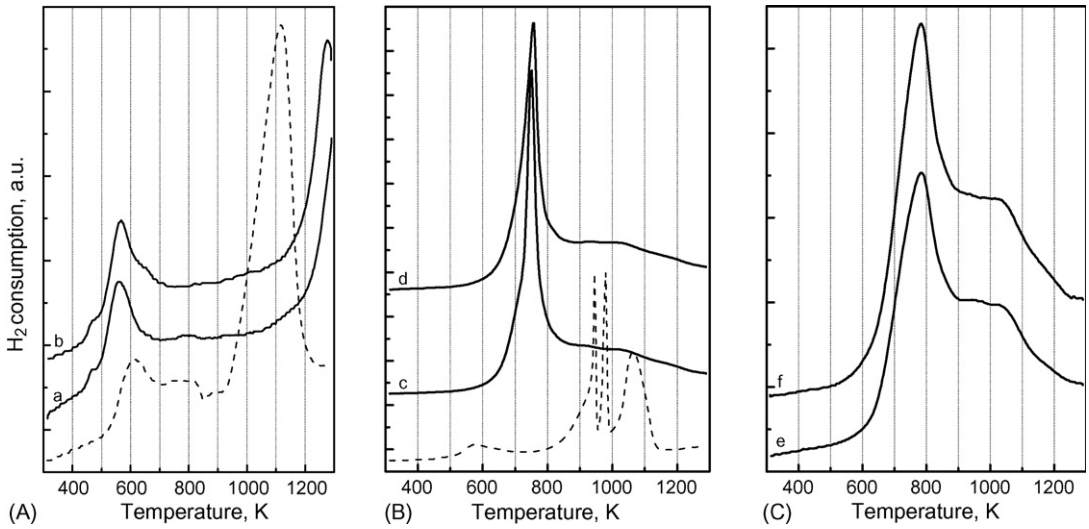

Fig. 2. H_2-TPR profiles of (A) supported niobia materials, (B) alumina supported vanadium oxide and (C) vanadia-niobia supported catalysts. The profiles represent the following materials: (a) 4Nb/Al, (b) 6Nb/Al, (c) 4V/Al, (d) 6V/Al, (e) 4VNb/Al and (f) 6VNb/Al. The profiles marked by dash line on A and B described the reduction of Nb_2O_5 and V_2O_5, respectively.

Fig. 2B shows the TPR profiles of alumina-supported vanadia. The 4V/Al and 6V/Al materials (profiles c and d) shift to 100 K higher the onset reduction temperature compared to bulk vanadium oxide (Table 1, $T_{o,red}$). This difference can be attributed to a strong interaction between surface vanadium species and the alumina. The reduction of bulk V_2O_5 occurs at higher temperature than alumina supported vanadia due to increased diffusion limitation in bulk V_2O_5 [18]. The reduction profiles for bulk vanadia reported in literature show differences, probably because of the origin of the oxide precursor, level of the impurities and the reduction conditions [18,19]. The three main peaks on the TPR profile of bulk V_2O_5 were ascribed to the reduction in different steps: $V_2O_5 \rightarrow V_6O_{13} \rightarrow V_2O_4 \rightarrow V_2O_3$ [14,20,21]. It should be noted that the structure of supported vanadium oxide on alumina is completely different to that of bulk vanadia. The single reduction peak appears associated to a reduction from surface V^{5+} to surface V^{3+} species, which apparently integrate in the alumina support lattice, according to EXAFS analyses [22].

The V/Al reduction profiles exhibit a sharp peak near 750 K and a tailing of the signal above this temperature. The sharp peak can be due to the reduction of surface vanadium oxide species [18,19,23]. The broad reduction features are evident at higher temperatures (Table 1, T_{M2} and T_{M3}), these are typically assigned to the reduction of bulk-like species, which may exist in a highly dispersed state on the support surface [4,18,19,23], they may also be due to strongly-interacting vanadia-alumina species-precursor for mixed V–Al–O phases (e.g., $AlVO_4$).

The TPR profiles of VNb/Al system (Fig. 2C, e and f) exhibit features that roughly resemble those of alumina-supported vanadia (T_{max} values in Table 1). However, the onset reduction temperature is closer to that of alumina-supported niobia (Table 1). Thus, mixed vanadia-niobia on alumina appears to share reduction characteristics from both components. Both profiles show broad peak with the same maximum at 784 K (T_{M2}), which probably origins from the reduction of the surface vanadium oxide species. The presence of Nb shifts the vanadium reduction maximum to higher temperature. The stabilizing role of niobium was described earlier in literature [24].

The TPO analyses of the alumina supported vanadia and niobia catalysts are presented in Table 2 (TPO profiles not shown here for the brevity). It should be noted that temperature-programmed oxidation was performed after the H_2-TPR experiments. All samples were treated during the reduction conditions up to 1323 K. These conditions may lead to the formation of crystalline phases. All catalysts exhibit similar onset oxidation temperature ($T_{o,oxy}$), near 320 K. 6Nb/Al and 6V/Al show four oxidation maxima (T_{M1}, T_{M2}, T_{M3}, T_{M4}),

Table 1
Summary of temperature-programmed reduction results

Catalyst	$T_{o,red}$ (K)[a]	T_{M1} (K)	T_{M2} (K)	T_{M3} (K)	T_{M4} (K)
4Nb/Al	315	496	558	795	
6Nb/Al	395	473	567	650	1278
4V/Al	550		751	928	1030
6V/Al	515		756	935	1033
4VNb/Al	360		784	952	1027
6VNb/Al	355		783		1025
Nb_2O_5	335		614	772	1117
V_2O_5	453	575	945	979	1064

[a] The onset reduction temperature values were estimated as a beginning of H_2 consumption growth compare to the baseline.

Table 2
The oxidation temperatures (TPO) of the alumina supported catalysts

Catalyst	$T_{o,oxy}$ (K)	T_{M1} (K)	T_{M2} (K)	T_{M3} (K)	T_{M4} (K)
4Nb/Al	317	607			1003
6Nb/Al	325	616	827	933	1004
4V/Al	322		827	918	1001
6V/Al	316	734	824	888	994
4VNb/Al	324		827		977
6VNb/Al	315			937	1012

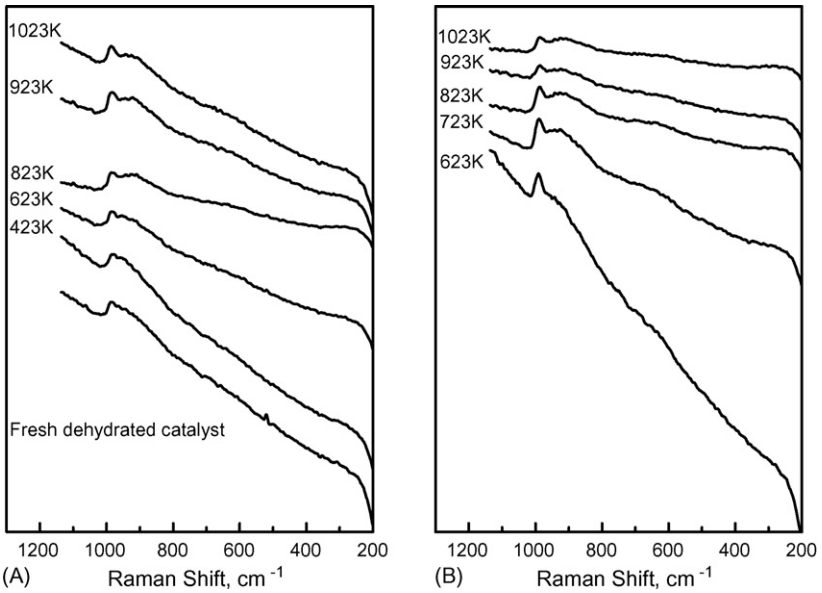

Fig. 3. Selected Raman spectra of the 6Nb/Al catalyst during the TPR-Raman of fresh sample (A) and during the TPO-Raman of the reduced sample (B).

whereas the remaining samples exhibit only two or three. Therefore, it is expected a higher variety of species at higher coverage values.

In situ temperature-programmed Raman (TP-Raman) experiments allow observing the structural changes of the surface oxide species under reducing/oxidizing environments. The materials with the same chemical composition exhibit similar trends during TPR/TPO. The 4Nb/Al (spectra not presented) and 6Nb/Al samples do not possess the Raman features of crystalline Nb_2O_5 (TT) phase (bands at ~238, 315 and 702 cm^{-1}) or $AlNbO_4$ (major bands at ~930, 420 and 240 cm^{-1}) [15,25]. However, there is a fluorescence background that cannot be removed by calcination. It may be due to an incipient Al–Nb interaction at the interface since some mixed Al–Nb–O phases exhibit luminescence [26]. Fig. 3 shows representative Raman spectra of the 6Nb/Al catalyst during the TPR and TPO cycles. The fresh dehydrated sample exhibits a Raman band at 984 cm^{-1} which is assigned to the Nb=O stretching mode in highly distorted surface NbO_6 octahedra on alumina [27,28]. The second band in the region 960–840 cm^{-1} is not well developed in this spectrum—probably due to fluorescence interference; it has been assigned to bridging O–Nb–O bond [27]. The Raman bands near 980 and 928 cm^{-1} become better resolved and the background fluorescence decreases above 600 K. Apparently, surface NbO_6 octahedra on alumina are not affected by this reduction. This may be indicative of the reduction of some ill-defined Al–Nb phase, in agreement with the first reduction peak and the fact that some mixed Nb–Al–O phase exhibit luminescence [26]. During the reduction process, no other significant changes are evident up to 1023 K (Fig. 3A). The

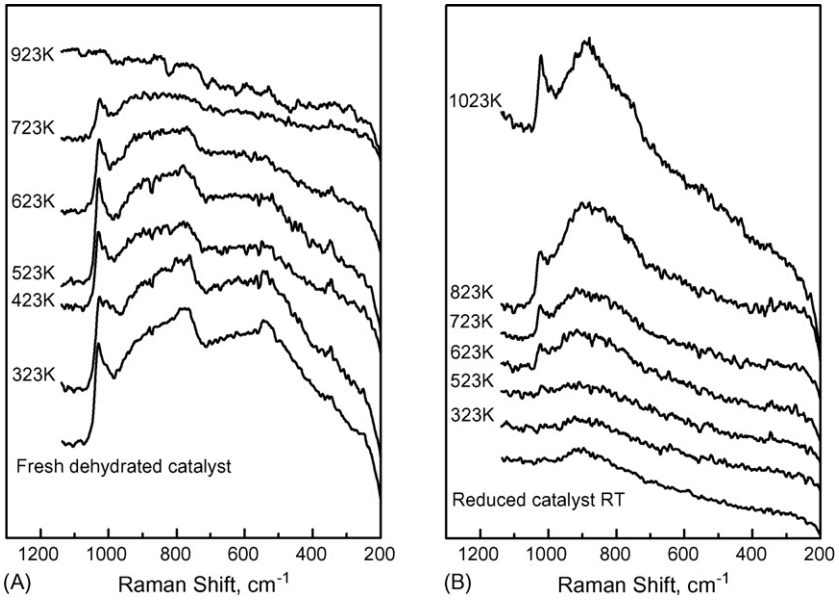

Fig. 4. TPR/TPO selected Raman spectra of the 6V/Al material during (A) reduction of fresh sample and (B) oxidation of the reduced sample.

TPO-Raman did not reveal significant changes in the spectra, but an additional decrease of fluorescence. Therefore, the reduction would remove bridging Nb–O–Al bonds associated to an Nb–Al interface, thus minimizing fluorescence, while dispersed niobium oxide species would remain unaffected.

The alumina supported vanadium oxide species below monolayer coverage do not exhibit the Raman features of crystalline V_2O_5 (994, 703, 527, 485, 405, 305, 282 and 144 cm^{-1}). Dehydrated 4V/Al exhibits bands at 1027, 865, 767, 535 and 345 cm^{-1} (not shown). They are assigned to a stretching mode of terminal V=O bond (1027 cm^{-1}) and bridging V–O–V functionalities. The stretching mode of V–O–V bond and bending mode of V–O bonds are responsible for the bands at 865, 767 and 540 cm^{-1} (broad) and at 345 cm^{-1}, respectively [29–32]. Similarly, fresh dehydrated 6V/Al possesses Raman bands at 1029, 880, 776, 625, 539, 340 and 249 cm^{-1} (Fig. 4A). This spectrum shows two more bands attributed to stretching mode of V–O–V bond and bending mode of V–O–V bond, in comparison with a spectrum of 4V/Al, this suggests a higher degree of polymerization. The terminal V=O and V–O–V Raman bands in 6VAl shift to higher wavenumber suggesting a higher polymerization degree of surface vanadia species than in 4V/Al [32]. The Raman spectra did not show the presence of VO_2 or V_6O_{13} phases [33]. 6V/Al exhibits small Raman shoulders that suggest the incipient formation $AlVO_4$ [23], in line with X-ray analyses.

During the TPR-Raman experiments, the intensity of the Raman bands related to the polymeric vanadium oxide species decreases faster with temperature than the band of terminal V=O bond. It suggests that the polymeric species undergo easier reduction, which is consistent with *in situ* UV–vis studies of alumina-supported oxides under reducing conditions [34]. The Raman bands of surface vanadium oxide species disappear at 923 K for 4V/Al and 6V/Al. The TPR-Raman experiment was performed up to 1023 K (spectrum not shown due to blackbody radiation). The comparison between conventional H_2-TPR and TPR-Raman results allows presuming that at this temperature most of vanadium oxide supported on alumina is reduced (V^{3+}). The reduced 4V/Al and 6V/Al exhibit a weak band at 904 cm^{-1}. This band is not visible at the reduction temperature due to black body radiation, but can be observed after cooling the reduced sample (reduced catalyst at room temperature in Fig. 4B). A weak shoulder at 991 cm^{-1} for 4V/Al and 1009 cm^{-1} for 6V/Al is also evident. During the TPO-Raman experiment, polymeric vanadium surface oxide species appear increasingly important compared to the fresh catalyst. The relative intensity of the Raman bands related to polymeric species grow faster, in agreement with the loss of dispersion of supported vanadia species upon reduction [2,23,35].

The Raman spectrum of 6VNb/Al (Fig. 5) is richer in bands than the 4VNb/Al (not shown) one. It should be noted that the V + Nb mixed oxides concentration is half as much in the comparison with 6VNb/Al. However, there are two shoulders in the 900–1030 cm^{-1} region. The first at 1025 cm^{-1} is associated with the terminal V=O bond and the second at 989 cm^{-1} with Nb=O bond [27,28]. The mono-oxo Nb=O stretching mode (980 cm^{-1}) is not visible on 6VNb/Al sample (Fig. 5A) since the stronger Raman bands of the vanadium oxide species must overshadow the weak Raman bands of the niobium oxide species [24]. The Raman band ca. 900 cm^{-1} can originate from the stretching mode of V–O–V bond or the stretching mode in polymerized Nb–O–Nb bonds (Fig. 5A) [27,30]. For VNb/Al, the Raman bands at 200–300 cm^{-1} are assigned to the angle deformation modes of Nb–O–Nb and bridging Nb–O–Nb bonds [15]. The Raman modes near 600–700 cm^{-1} have been assigned to distorted NbO_6 structures [27]. The spectrum of dehydrated 6VNb/Al sample possesses a small shoulder at 781 cm^{-1}, which is normally assigned to the crystalline $NbVO_5$ phase [36]. However, the X-ray diffraction pattern of this catalyst does not indicate any crystalline phase. In addition, this Raman band disappears upon hydration (not shown) and these crystalline phases are not sensitive to hydration. It appears that

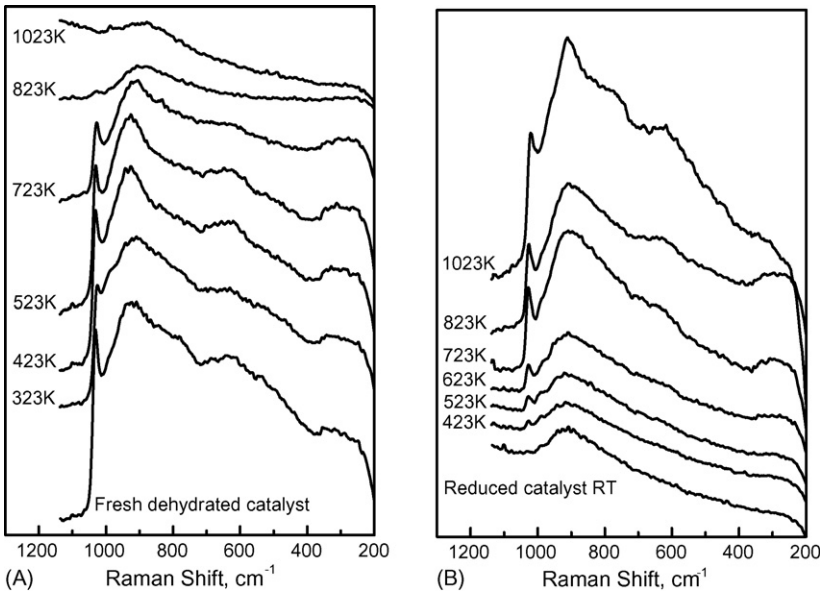

Fig. 5. TPR/TPO selected Raman spectra of the 6VNb/Al material during (A) reduction of fresh sample and (B) oxidation of the reduced sample.

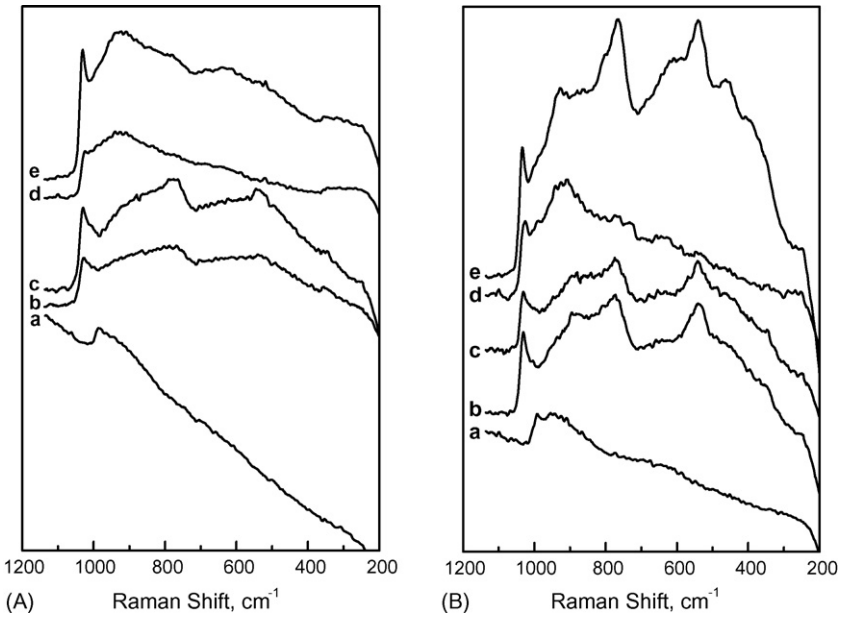

Fig. 6. Raman spectra of dehydrated alumina supported oxides before (A, 323 K) and after (B, RT) TPR/TPO cycle: (a) 6Nb/Al, (b) 4V/Al, (c) 6V/Al, (d) 4VNb/Al and (e) 6VNb/Al.

the band at 781 cm^{-1} and the Raman bands in the 450–600 cm^{-1} are related to the polymeric V–O–V functionality. Raman modes weaken during the reduction process. However, unlike Nb-free samples, it is difficult to determine which form reduces faster: the terminal V=O or the bridging V–O–V bond. The Raman bands of surface vanadium oxide species disappear at 923 K. After TPR-Raman experiment, the reduced samples exhibit the modes from niobium surface oxide species at 840 cm^{-1} for 4VNb/Al (not shown), and 985 and 910 cm^{-1} for 6VNb/Al (Fig. 5B). During the initial TPO stages, the surface niobium oxide species are visible; the progressive reoxidation of vanadium species yields the stronger Raman bands of vanadium oxide species. The reoxidized 4VNb/Al and 6VNb/Al samples exhibit stronger Raman bands at 920–990 cm^{-1}, underlining an increase in the polymerization degree of these samples.

Because of thermal broadening, the Raman bands at high temperatures may result less informative. The Raman spectra at room temperature of dehydrated alumina supported vanadium and/or niobium oxides before and after the TPR/TPO cycle are given in Fig. 6. The Raman bands shift towards higher wavenumber after the reduction/reoxidation cycle (Table 3), which underlines an increasing polymerization degree in the surface oxide species. Some of the spectra exhibit new bands. Such trend has also been reported for vanadia supported on alumina and on silica [2,23,35]. This phenomenon concerns also alumina supported niobium oxide. Niobium compounds exhibit lower mobility and reducibility. However, it appears that the TPR/TPO cycle conditions are enough to change the polymerization degree of niobia species. The Raman band at 647 cm^{-1} appears after the TPR/TPO cycle. The growth of its intensity reflects an increase in the polymerization degree in 6Nb/Al [27]. This would be consistent with a progressive removal of an incipient luminescent Al–Nb–O phase upon reduction. Subsequent oxidation would result in surface niobium oxide species,

Table 3
Summarized the Raman band before and after TPR/TPO cycle

Catalyst	Raman bands (cm^{-1})										
Fresh dehydrated catalyst, 323 K											
6Nb/Al[a]	984(m)	928(w)									
4V/Al	1027(s)	1015(w)	865(w)	767(m)		535(m)	345(w)				
6V/Al	1029(s)	1008(w)	880(w)	776(m)	625(w)	539(m)	340(w)	249(w)			
4VNb/Al	1024(w)	989(w)	926(m)	837(w)	770(w)	645(m)		343(w)	312(w)	268(w)	
6VNb/Al	1031(s)		924(m)	861(w)	781(w)	627(m)	537(w)		312(w)		
Dehydrated catalyst after TPR/TPO cycle, RT											
6Nb/Al	991(m)	943(m)	647(w)								
4V/Al	1030(s)	1006(w)	894(m)	773(s)	640(w)	538(s)		350(w)	251(w)		
6V/Al	1032(s)	1003(w)	894(m)	770(s)	631(w)	541(s)	466(w)	347(w)	251(w)		
4VNb/Al	1026(m)	989(w)	929(s)	879(w)	767(m)	731(m)	641(m)	543(w)	345(w)	288(w)	268(w)
6VNb/Al	1034(s)	926(m)	862(w)	801(w)	766(s)	608(m)	540(s)	463(m)	408(w)		248(w)

[a] Raman bands dehydrated catalyst at 673 K.

like those described by Wachs and co-workers [27]. The relative intensity of the Raman bands also undergoes changes. It particularly applies to the Raman modes attributed to the polymeric M–O–M functionality, which grows stronger in all vanadium-containing catalysts. In addition, 6V/Al also broadens the band at 1032 cm^{-1}, which is associated to V=O vibration (Fig. 6B, c). This would be indicative of an increasing contribution of the V=O vibration of polymeric vanadia species.

4. Discussion

4.1. Alumina-supported niobium oxide

The reduction of bulk niobia exhibits two reduction maxima. The low-temperature (LT) reduction peak of Nb_2O_5 is very sensitive to experimental conditions and is not always present. Ziolek et al. [37] and Mendes et al. [38] did not observe any LT reduction maxima below the pre-treatment temperature (673 K). It seems that the nature of the gases used in pre-treatment affects TPR profile of niobium-containing materials. The application of inert gases (argon, helium) in combination with higher temperature can lead to the partial reduction of easier reducible species before TPR. For alumina-supported niobia, the X-ray analyses suggest that niobium oxide species are well dispersed on Al_2O_3, or at least crystalline phases are not large enough to generate a diffraction pattern. The temperature-programmed reduction technique allows estimating the reducibility of niobium catalyst. *Addition of niobia to alumina results in two opposite trends*. Nb/Al_2O_3 exhibits reduction of the niobium species in two ranges: at low (560 K) and at high temperature (above 1000 K). The low-temperature reduction peak is below that of bulk niobia and the high-temperature one is above that of bulk niobia. No bulk niobia is present in this system, only surface niobia interacting with alumina. A phase that is not observed by XRD or Raman spectroscopy reduces near 560 K. The formation of this reducible phase strongly depends on the applied pre-treatment conditions. In the low-temperature region, the TPR profile shows broad and small peaks with maxima at 558 and 567 K. A similar feature was detected for bulk Nb_2O_5 during reduction. This peak suggests the reduction of niobium species, closely interacting with alumina—an incipient V-Nb-O phase, which reduces more easily. The nature of this phase is not clear. There appears to be a strong interaction between niobium and aluminum oxide support; it makes sense to believe that it would lead to an incipient Al–Nb–O phase, which is luminescent. Indirect evidence is provided, since it would account for the intense fluorescence that is not quenched by calcination. The surface niobium oxide species reduce above 1000 K; their reducibility depended on Nb loading. The growth of reducibility with niobium loading resulted from the formation of larger niobia aggregates that minimize the interface. Mendes et al. [38] pointed out that the nature of the precursor affected the reduction of niobium oxide species. The system prepared from the niobium oxalate exhibit higher reducibility than that prepared from ammonium niobium oxalate. The growth of the Raman band near 650 cm^{-1} underlines an increase in the polymerization degree [27] after TPR/TPO cycle.

4.2. Alumina-supported vanadium oxide

Alumina-supported vanadium oxide catalysts are essentially dispersed, according to Raman and XRD analyses. XRD reveals that 6V/Al possesses an additional crystalline phase, $AlVO_4$. The pattern is weak and it cannot tell between other phases exhibiting similar patterns, like V_6O_{13} and VO_2. The application of Raman spectroscopy excluded the existence of VO_2 or V_6O_{13} phases in this material [33]. These bands are weak compared to those of V^{5+} species. $AlVO_4$ can be detected more easily by Raman spectroscopy. The Raman spectrum of 6V/Al exhibited small shoulders at 970 and 1003 cm^{-1}, which confirm the presence of some $AlVO_4$ [23]. A small shoulder at 1009 cm^{-1} was still visible even after the reduction process. It suggests the strong interaction between this vanadium species and alumina support, and is consistent with the lower reducibility of $AlVO_4$. In any case, $AlVO_4$ is not much representative of the whole sample. The modification of the alumina with $VOSO_4$ leaded to the presence of both vanadium oxide species and sulphate species on the surface. The sulphate preferentially coordinates with the oxide support rather than the surface vanadia species [39,40]. The Raman bands of surface vanadium oxide species show no effect due to sulphate species. The surface sulphate species titrate only the most basic hydroxyls, while surface vanadium oxide species titrate both basic and neutral support hydroxyls. The tridentate sulphates species under dehydrated conditions are converted into protonated bidentate surface species under water vapour [39,41]. This process generates a moderately acidic S–O–H group, which increases the Brønsted acidity of the system [39,41]. H_2-TPR profiles of alumina supported vanadium oxide species exhibit sharp reduction peaks, characteristic of surface vanadium oxide species on alumina. The existence of isolated and polymeric VO_x on the support broadens the reduction peak. Moreover the rising of vanadium content increases the reduction peak at low temperature [19]. It is not well understood how the presence of polymeric and isolated vanadium oxide species affect the reduction profiles [18,23,42], but TPR-Raman experiments reveal that polymeric V–O–V bonds reduce faster than isolated species [43]; this trend is actually confirmed by *in situ* UV–vis studies [33,43]. The reduction peak around 1000 K is attributed to the reduction of bulk-like vanadia species, which may exist in a highly dispersed state on the support surface [4,18,19,23]. Alumina-supported V^{5+} species reduce to V^{3+}. Ruitenbeek et al. [22] suggest that V^{3+} ions are not stable on the surface of alumina and they immediately migrate to an Al^{3+} octahedral position after reduction. The reduced V/Al_2O_3 materials exhibit Raman bands at 900 and 1000 cm^{-1} (Fig. 4); these bands probably correspond to V^{3+}–O–Al^{3+} bonds of surface reduced vanadia species. V^{5+}–O–Al^{3+} stretching vibrations have been reported for V–O–Al bonds in $AlVO_4$ [44]. The V–O–Al bonds are weak in $AlVO_4$, however, these maybe stronger for reduced vanadia on alumina since the V^{3+}–O–Al^{3+} bond is less polarized and should shift. Upon reoxidation, a clear shift of the Raman bands suggests an increase in the polymerization degree of the surface vanadium oxide species. Such trend has consistently been observed for supported vanadium oxide under reducing conditions [2,35].

4.3. Alumina-supported vanadium-niobium oxide system

The XRD analyses of VNb/Al catalysts did not show any crystalline mixed oxides phase, even when the system V-Nb-Al-O may form ternary compounds [45]. Binary phases (V_2O_5-Nb_2O_5, V_2O_5-Al_2O_3 and Nb_2O_5-Al_2O_3) may form in these catalysts. Resini et al. [9] observed $NbVO_5$, VNb_9O_{25} crystalline phases for V-Nb/SiO_2 catalyst both in the XRD pattern and in the Raman spectra. However, silica interacts very weakly with supported oxides and promotes the interaction among the cations at its surface. Other supports like alumina, titania or zirconia, among others, interact strongly with the supported phase. For our alumina-supported catalysts, X-ray diffraction did not show any mixed vanadium-niobium oxides; in addition, VNb/Al_2O_3 systems did not exhibit any Raman bands corresponding to crystalline phases described in the literature ($V_4Nb_{18}O_{55}$, $NbVO_5$ and VNb_9O_{25}) [9,15,24]. Alumina-supported mixed metal oxides below monolayer coverage did not exhibit Raman bands from crystalline phases during the reduction/oxidation cycle. The Raman spectra are dominated by the stronger bands of the vanadium oxide species, which overshadow the weaker Raman bands of the niobium oxide species [24]. During the reduction process, the intensity of the Raman band corresponding to V=O and V–O–V bonds of surface vanadium oxide species decrease up to 423 K. The intense Raman band at ~1027 cm^{-1} was visible above this temperature. It suggests that polymeric vanadium oxide species reduce faster. Upon TPR/TPO cycles, the mixed vanadia-niobia catalysts on alumina exhibit a higher degree of polymerization. The data suggest that mainly vanadium oxide species undergo reduction under our experimental conditions. However the *maximum reduction temperature was achieved at a higher temperature than the vanadium-free catalysts*. Thus, Nb retards the reducibility of surface vanadium oxide species. Wachs et al. report that niobium has a stabilizing effect on the V_2O_5/TiO_2 system: it retarded the formation of crystalline V_2O_5 during calcinations [24]. The reduction of supported vanadium species is favored by the aggregation of dispersed vanadium oxide species into crystalline V_2O_5 [23]. The reduction of surface vanadia is facilitated by oxygen-sharing between reduced surface vanadia species that, in turn, promotes the aggregation of dispersed vanadia species [2]. Therefore, the presence of Nb species among the surface vanadia species would negatively affect the reduction of vanadia, and thus account for the broadening and overall shift to higher temperature of the reduction profiles.

5. Conclusions

- The supported mixed metal oxide (V_2O_5, Nb_2O_5) do not form the crystalline phases on the alumina support surface below monolayer coverage, but essentially remain dispersed as surface vanadia and surface niobia species. There is evidence that a small fraction of vanadia reacts with alumina support to form $AlVO_4$ and indirect evidence that Nb–Al–O phases form.
- The reduction profile of alumina-supported vanadia is different to that of bulk V_2O_5 since its structure is different. Reduced vanadia on alumina exhibit a Raman band near 900 cm^{-1} that may correspond to the V^{3+}–O–Al^{3+} bond vibration.
- The polymeric surface vanadia species reduce faster than the isolated ones.
- Niobia on alumina is less reducible; however, a fraction of niobia is highly reducible (623 K), this is probably due to the presence of Nb species strongly interacting with alumina as an incipient Al–Nb–O phase. These phases are luminescent, which would account for the fluorescence background and its removal above 623 K. Most of the niobia phase would reduce at significantly higher temperatures (above 1100 K). Thus, surface niobium oxide species remain present after the TPR-Raman run up to 1023 K, which is confirmed by its Raman bands at 980 and 935 cm^{-1}.
- Niobia does not form phases with vanadia below monolayer coverage on alumina but it does affect the reducibility characteristics of surface vanadia species.
- The TPR/TPO cycles increase the polymerization degree of the surface vanadium and niobium oxide species on alumina.

Acknowledgements

Spanish Ministry of Education and Science (Becas de Doctores y Tecnólogos, MEC, SB2003-0179) is acknowledged for postdoctoral fellowship for AEL. The NATO ESP.NR. NRCLG 981857 grant support is acknowledged. SASOL, Inorganic Specialty Chemicals, is acknowledged for providing alumina support.

References

[1] I.W.C.E. Arends, R.A. Sheldon, M. Wallau, U. Schuchard, Angew. Chem. Int. Ed. Engl. 36 (1997) 1144.
[2] M.A. Bañares, J.H. Cardoso, F. Agulló-Rueda, J.M. Correa-Bueno, J.L.G. Fierro, Catal. Lett. 64 (2000) 191.
[3] P. Concepción, M.T. Navarro, T. Blasco, J.M. Lopez Nieto, B. Panzacchi, F. Rey, Catal. Today 96 (2004) 179.
[4] S. Shylesh, A.P. Singh, J. Catal. 228 (2004) 333.
[5] M.O. Guerrero, J.L.G. Fierro, M.A. Bañares, Catal. Today 78 (2003) 387.
[6] M.A. Bañares, S.J. Khatib, Catal. Today 96 (2004) 251.
[7] P. Viparelli, P. Ciambelli, J.C. Volta, J.M. Herrmann, Appl. Catal. A 182 (1999) 165.
[8] P. Viparelli, P. Ciambelli, L. Lisi, G. Ruoppolo, G. Russo, J.C. Volta, Appl. Catal. A 184 (1999) 291.
[9] C. Resini, M. Panizza, F. Raccoli, M. Fadda, M.M. Carnasciali, G. Busca, E. Fernandez Lopez, V. Sanchez Escribano, Appl. Catal. A Gen. 251 (2003) 29.
[10] M. Ziolek, A. Lewandowska, M. Renn, I. Nowak, Stud. Surf. Sci. Catal. 154 (2004) 2610.
[11] K. Tanabe, Catal. Today 78 (2003) 65.
[12] M. Ziolek, Catal. Today 78 (2003) 47.
[13] R.H.H. Smits, K. Seshan, H. Leemreize, J.R.H. Ross, Catal. Today 16 (1993) 513.
[14] K.V.R. Chary, G. Kishan, C.P. Kumar, G.V. Sagar, J.W. Niemantsverdriet, Appl. Catal. A Gen. 245 (2003) 303.
[15] Z. Zhao, X. Gao, I.E. Wachs, J. Phys. Chem. B 107 (2003) 6333.
[16] M. Catauro, C. Pagliuca, L. Lisi, G. Ruoppolo, Thermochim. Acta 381 (2002) 65.
[17] R.H.H. Smits, K. Seshan, J.R.H. Ross, Catalytic selective oxidation, in: S.T. Oyama, J.W. Hightower (Eds.), ACS Symposium Series, vol. 523, 1993, p. 380.

[18] E.P. Reddy, R.S. Varma, J. Catal. 221 (2004) 93.
[19] N.R. Shiju, M. Anilkumar, S.P. Mirajkar, C.S. Gopinath, B.S. Rao, C.V. Satyanarayana, J. Catal. 230 (2005) 484.
[20] R.S.G. Ferreira, P.G.P. Oliveira, F.B. Noronha, Appl. Catal. B Environ. 29 (2001) 275.
[21] M.M. Koranne, J.G. Goodwin, G. Marcelin, J. Catal. 148 (1994) 369.
[22] M. Ruitenbeek, A.J. van Dillen, F.M.F. de Groot, I.E. Wachs, J.W. Geus, D.C. Koningsberger, Top. Catal. 10 (2000) 241.
[23] J.M. Kanervo, M.E. Harlin, A.O.I. Krause, M.A. Bañares, Catal. Today 78 (2003) 171.
[24] I.E. Wachs, J.-M. Jehng, F.D. Hardcastle, Solid State Ionics 32/33 (1989) 904.
[25] J.-M. Jehng, I.E. Wachs, Chem. Mater. 3 (1991) 100.
[26] G. Blasse, R.U.E. 'T Lam, J. Solid State Chem. 25 (1978) 77.
[27] L.J. Burcham, J. Datka, I.E. Wachs, J. Phys. Chem. B 103 (1999) 6015.
[28] J.-M. Jehng, I.E. Wachs, J. Phys. Chem. 95 (1991) 7373.
[29] G.T. Went, S.T. Oyama, A.T. Bell, J. Phys. Chem. 94 (1990) 4240.
[30] M.A. Bañares, I.E. Wachs, J. Raman Spectrosc. 33 (2002) 359.
[31] J.-M. Jehng, G. Deo, B.M. Weckhuysen, I.E. Wachs, J. Mol. Catal. A Chem. 110 (1996) 41.
[32] L.J. Burcham, G. Deo, X. Gao, I.E. Wachs, Top. Catal. 11/12 (2000) 85.
[33] X.J. Wang, H.D. Li, Y.J. Fei, X. Wang, Y.Y. Xiong, Y.X. Nie, K.A. Feng, Appl. Surf. Sci. 177 (2001) 8.
[34] X. Gao, M.A. Bañares, I.E. Wachs, J. Catal. 188 (1999) 325.
[35] S.B. Xie, E. Iglesia, A.T. Bell, Langmuir 16 (2000) 7162.
[36] M. Sarzi-Amade, S. Morseli, P. Moggi, A. Maione, P. Ruiz, M. Devillers, Appl. Catal. A Gen. 284 (2005) 11.
[37] M. Ziolek, I. Sobczak, A. Lewandowska, I. Nowak, P. Decyk, M. Renn, B. Jankowska, Catal. Today 70 (2001) 169.
[38] F.M.T. Mendes, C.A. Perez, R.R. Soares, F.B. Noronha, M. Schmal, Catal. Today 78 (2003) 449.
[39] J.P. Dunn, H.G. Stenger Jr., I.E. Wachs, Catal. Today 51 (1999) 301.
[40] J.P. Dunn, J.-M. Jehng, D.S. Kim, L.E. Briand, H.G. Stenger, I.E. Wachs, J. Phys. Chem. B 102 (1998) 6212.
[41] O. Saur, M. Bensitel, A.B. Mohammed Saad, J.C. Lavalley, C.P. Tripp, B.A. Morrow, J. Catal. 99 (1986) 104.
[42] F. Arena, F. Frusteri, A. Parmaliana, Appl. Catal. A Gen. 176 (1999) 189.
[43] M.A. Bañares, M.V. Martínez-Huerta, X. Gao, J.L.G. Fierro, I.E. Wachs, Catal. Today 61 (2000) 295.
[44] H. Tian, I.E. Wachs, L. Briand, J. Phys. Chem. B 109 (2005) 23491.
[45] M.G. Zuev, Russ. Chem. Rev. 69 (2000) 551.